Quaternary Research 83 (2015) 370–377

Contents lists available at ScienceDirect

Quaternary Research

journal homepage: www.elsevier.com/locate/yqres

Hydroclimate implications of thermocline variability in the southern South China Sea over the past 180,000 yr

Liang Dong [a], Li Li [a,*], Qianyu Li [a,b,*], Hui Wang [a], Chuanlun L. Zhang [a]

[a] State Key Laboratory of Marine Geology, Tongji University, Shanghai 200092, China
[b] School of Earth and Environment Sciences, University of Adelaide, SA 5005, Australia

ARTICLE INFO

Article history:
Received 10 February 2014
Available online 23 January 2015

Keywords:
$U^{K'}_{37}$
TEX $^{H}_{86}$
Depth of thermocline (DOT)
East Asian Monsoon (EAM)
South China Sea (SCS)
El Niño-Southern Oscillation (ENSO)

ABSTRACT

Based on core-top calibration, the TEX $^{H}_{86}$-derived temperature has been considered as representing subsurface sea temperature (SSST), and the difference between the $U^{K'}_{37}$-derived sea-surface temperature (SST) and the TEX $^{H}_{86}$-derived SSST can be used to reflect the depth of thermocline (DOT) in the South China Sea region (Jia et al., 2012). We evaluated the DOT dynamics in late Quaternary records using this approach on paired analysis of samples from core MD05-2896/7 in the southern South China Sea. The reconstructed DOT over the last 180,000 yr (180 ka) displays a shoaling trend in glacial periods, which may be attributed to the strengthened cyclonic gyre by the enhanced East Asian winter monsoon and Walker circulation with prominent La Niña-like state, and vice versa in interglacial periods corresponding to reduced winter monsoon with enhanced El Niño-like state. These upper-water thermal variations testify that enhanced winter monsoon was the direct cause of an uplifted local thermocline during glacial or La Niña-like states with strengthened cyclonic gyre due to positive wind stress curl in the southern South China Sea. Our results provide insights into the relationship between monsoon and ENSO on both glacial and millennial time scales.

© 2014 University of Washington. Published by Elsevier Inc. All rights reserved.

Introduction

By redistributing heat and moisture between the Asian continent and the low-latitude Pacific Ocean, the oceanic and atmospheric circulations determine the basic patterns of temperature, precipitation and vegetation in this region. At the center of land–sea interaction between Asia and Pacific, the South China Sea (SCS) is a unique location for paleoclimate and paleoceanographic studies (Wang and Li, 2009). Its upper-water structure, especially the depth of thermocline (DOT), is of particular significance in reflecting the thermal evolution of the SCS influenced by the western Pacific warm pool (WPWP) and East Asian monsoon (EAM), and probably also by El Niño-Southern Oscillation (ENSO) cycles.

For the modern relationship between EAM and ENSO, latest research shows that El Niño events are associated with an especially weak East Asian winter monsoon (EAWM) when the ENSO-EAWM relationship enhances, and that the southward motion of the Walker circulation reduces the impacts of ENSO on the EAWM during their low correlation periods (He and Wang, 2013, and references therein). However, work on the relationship between EAM and ENSO-like states over glacial–interglacial cycles is sparse. Seasonal (such as monsoon) or inter-annual (such as ENSO) climatic phenomena over glacial cycles have even been attempted based on centenary or lower sampling resolution (Beaufort et al., 2003), and for some cases whether these proposed climatic phenomena can be recognized on the glacial–interglacial time scale is unclear. Accordingly, interpretations of past ENSO-like phenomena based on geologic evidence remain quite diverse. For example, while some studies support El Niño dominance during global deglaciation, others endorse La Niña dominance for the same period (Andreasen et al., 2001; Beaufort et al., 2001; Koutavas and Joanides, 2012; Koutavas et al., 2002, Koutavas et al., 2006; Shaari et al., 2013, 2014; Stott et al., 2002; Tudhope et al., 2001).

Until now, most of our knowledge about the East Asian summer monsoon (EASM) relies heavily on stalagmite $\delta^{18}O$ records (e.g., Wang et al., 2001; Wang et al., 2008), while EAWM variability has been studied in records of grain-size changes in loess sequence (Ding et al., 2002; Guo et al., 2009) and diatom assemblages in lake sediments (Wang et al., 2012). Although many marine proxies have been proposed, their reliability is constantly under debate due to their indirect responses to monsoons (e.g., Huang and Tian, 2012; Tian et al., 2010; Wang et al., 2005). For example, it has been found that monsoon variability affects the DOT, as stronger winds may cause upwelling and subsequently raise the DOT. However, DOT may be also affected by ENSO, as the El Niño state often associates with a lifted DOT in the WPWP (Picaut et al., 1996). DOT variability on orbital and sub-orbital scales can be

* Corresponding authors at: State Key Laboratory of Marine Geology, Tongji University, Shanghai 200092, China. Fax: +86 21 65988808.
E-mail addresses: lilitju@tongji.edu.cn (L. Li), qli01@tongji.edu.cn (Q. Li).

http://dx.doi.org/10.1016/j.yqres.2014.12.003
0033-5894/© 2014 University of Washington. Published by Elsevier Inc. All rights reserved.

https://doi.org/10.1016/j.yqres.2014.12.003 Published online by Cambridge University Press

inferred by using proxies such as planktonic foraminifer assemblages, transfer functions, $\delta^{18}O$ gradient between surface and sub-surface planktonic foraminifers, and temperature difference between surface (e.g., $U^{K'}_{37}$; Mg/Ca) and subsurface (e.g., Mg/Ca; TEX $^{H}_{86}$) proxies (Jian et al., 2000a,b; Li et al., 2013; Ravelo and Fairbanks, 1992; Steinke et al., 2010; Steinke et al., 2011; Tian et al., 2005). Previous studies indicate that the $\delta^{18}O$ difference between subsurface planktonic foraminifer *Pulleniatina obliquiloculata* and surface species *Globigerinoides ruber*, or $\Delta\ \delta^{18}O_{(P\text{-}G)}$, may be biased by the salinity effect (Steinke et al., 2010; Tian et al., 2005), but their inferred temperature difference, $\Delta T_{(P\text{-}G)}$, appears to reflect DOT variations more reliably than other parameters (Steinke et al., 2010).

Supported by core-top calibrations, Jia et al. (2012) found that the TEX $^{H}_{86}$-derived temperature can be used to represent the subsurface-sea temperature (SSST) in the SCS, and that the ΔT between the $U^{K'}_{37}$-derived and TEX $^{H}_{86}$-derived temperature can be used to reflect DOT variations, with high (low) ΔT values representing DOT shoaling (deepening). This concept has been used to establish the mixed layer depth (MLD) variations over the last 365 ka in the northern SCS, revealing a general pattern of the EAWM activity in the region (Li et al., 2013). In addition, a similar concept has been applied to reflect the evolution of Atlantic meridional overturning circulation (AMOC) in the tropical North Atlantic (Lopes dos Santos et al., 2010) and the upwelling history in the eastern equatorial Pacific (Shaari et al., 2013, 2014). In the southwestern SCS (Yamamoto et al., 2013), the ΔT differences between core MD97-2151 (Zhao et al., 2006) and other western Pacific sites have been used to infer the variation of the EAWM, revealing a probable cause of winter monsoon variability by inter-hemispheric heat balance.

To examine the possible impact of EAM and ENSO on the regional upper water structures over glacial–interglacial cycles, here we present high-resolution $U^{K'}_{37}$-derived SST and TEX $^{H}_{86}$-derived SSST records over the last 180 ka in a single sedimentary core recovered in the southern SCS. For comparison, we also calculated the SST gradient between the western and eastern equatorial Pacific to indicate the mean climatic state in the tropical area (cf. Lea et al., 2000). Our results demonstrate that the integrated application of $U^{K'}_{37}$- and TEX $^{H}_{86}$-derived temperatures can serve as an effective proxy for understanding of paleohydrodynamics affected by climate change and provide insights into the mechanism of interaction between EAM and ENSO-like states over glacial–interglacial cycles.

Study location and regional setting

Core MD05-2896/7 is located in the southern SCS, where the northeast wind prevails in winter and southwest wind in summer (Fig. 1). Lying about 200–400 km away from estuaries over the glacial–interglacial cycles, the core site has been constantly under the warm pool influence. The modern annual mean SST is about 28°C, with 1–2°C differences between summer and winter. Positive wind stress curl exists in the southwest of the SCS (around 5°N to 11°N and 111°E to 116°E) in winter due to the EAWM, whereas negative wind stress curl exists in summer due to the EASM. Consequently, the positive wind stress curl drives cyclonic circulation that results in a dome of the thermocline in winter, and the negative wind stress curl drives cyclonic circulation that results in a depression of the thermocline in summer (Fig. 2a). Due to the prevalent monsoon, sea-surface circulation changes seasonally with a cyclonic circulation prevailing in winter and an anti-cyclonic circulation in summer, respectively. In normal years (i.e., 2007–2008, Fig. 2b), there is a stable cyclonic cold eddy around MD05-2896/7, which is driven by the geostrophic current and the positive wind stress curl caused by the EAWM. However, the cyclonic cold eddy almost disappeared in the El Niño winter of 1997 (Fig. 2c) but enhanced considerably or even spread to the whole deep basin in the La Niña winter of 1998 (Fig. 2d).

Material and methods

Core description and age model

MD05-2897 (08°49.53′N, 111°26.51′E; water depth 1658 m; core length 30.98 m) was retrieved from the slope near the Sunda Shelf in the southern SCS (Fig. 1) during MD147-Marco-Polo Cruise in 2005 (Laj et al., 2005). The upper 2-m section was missing from this core, and as compensation we also analyzed the corresponding 0–2 m section of a nearby core MD05-2896 (08°49.05′N, 111°26.4699′E; water depth 1657 m; total core length 11.03 m). Noteworthy is that core MD05-2896 is mainly composed of homogeneous gray–green clay while core MD05-2897 mainly silty clay. The upper 2 m of core MD05-2896 and the upper 13 m of core MD05-2897 were sub-sampled every 8 cm for foraminifer oxygen isotope analysis and every 2 cm for organic matter analysis, respectively.

Benthic foraminifer *Cibicidoides wullerstorfi* (shell size > 400 μm) were picked for stable isotope analyses, as described by Huang and Tian (2012). Age models for core MD05-2896 (Tian et al., 2010) and for the upper part of MD05-2897 (Huang and Tian, 2012) were constrained by a set of planktonic foraminiferal ^{14}C ages. For the lower part of MD05-2897, the age model (Huang and Tian, 2012) was established through tuning the planktonic foraminiferal $\delta^{18}O$ to Chinese stalagmite $\delta^{18}O$ records (Wang et al., 2008) and tuning the benthic foraminiferal $\delta^{18}O$ record to the global benthic $\delta^{18}O$ stack LR04 (Lisiecki and Raymo, 2005). Consequently, the integrated upper 13 m sediment core (upper 2 m of MD05-2896 and 0.7–13 m of MD05-2897) represents deposition in the last ~175 ka, from MIS 6 to 1. Thus, the time resolution averages to ~1000 yr for the $\delta^{18}O$ samples and ~90-400 yr for the organic samples.

We measured unsaturated alkenone (mainly produced by haptophytes) and glycerol dialkyl glycerol tetraethers (GDGTs) (mainly produced by planktonic archaea) to calculate the $U^{K'}_{37}$ and TEX $^{H}_{86}$, respectively. Studies have demonstrated that haptophytes mainly dwells in the photic zone, whereas the planktonic archaea distributes in the whole water column (Karner et al., 2001) and reaches maximum abundance in the subsurface water (50-200 m) (Hu et al., 2011; Wuchter et al., 2005).

Extraction of archaeal lipids and LC-MS analysis

Firstly, about 5 g freeze-dried samples were extracted ultrasonically five times by dichloromethane/methanol (3:1, V/V), after adding internal standards. The total lipid extracts (TLEs) were separated into two parts. One part was concentrated for the archaeal lipid analysis following the method described by Hopmans et al. (2004) and Schouten et al. (2007). Detailed description can be found elsewhere (Wei et al., 2011). Briefly, separation was performed with a Prevail Cyano column (2.1 mm × 150 mm × 3 μm diameter; Grace, USA) on Agilent 1200 HPLC, maintaining at 30°C. Injection volume varied from 10 to 20 μl. GDGTs were eluted isocratically with 99% hexane and 1% propanol for 5 min, followed by a linear gradient to 1.8% propanol in 45 min with the flow rate at 0.2 ml/min. Detection was achieved using an Agilent 6460 triple-quadrupole mass spectrometer with atmospheric pressure chemical ionization (APCI) ion source via selected ion monitoring (SIM) of $[M+H]^+$ ions (in MS1). GDGTs were quantified by integration of the peak areas. GDGT-derived temperature index (TEX_{86} or TEX $^{H}_{86}$) was calculated based on the relative abundance of GDGTs. Over the years, multi-calibrations have been established for sea temperature reconstruction based on the archaeal lipids, providing critical information on hydroclimate evolution (Jia et al., 2012; Kim et al., 2008, Kim et al., 2010; Liu et al., 2009; Schouten et al., 2002).

TEX_{86} is defined as $\frac{[GDGT-2]+[GDGT-3]+[Cren']}{[GDGT-1]+[GDGT-2]+[GDGT-3]+[Cren']}$, and TEX $^{H}_{86}$ = $\log TEX_{86}$. For SST calculation, we follow the calibration established by Kim et al. (2010): SST = 68.4 × TEX $^{H}_{86}$ + 38.6 (r^2 0.87, n = 255,

https://doi.org/10.1016/j.yqres.2014.12.003 Published online by Cambridge University Press

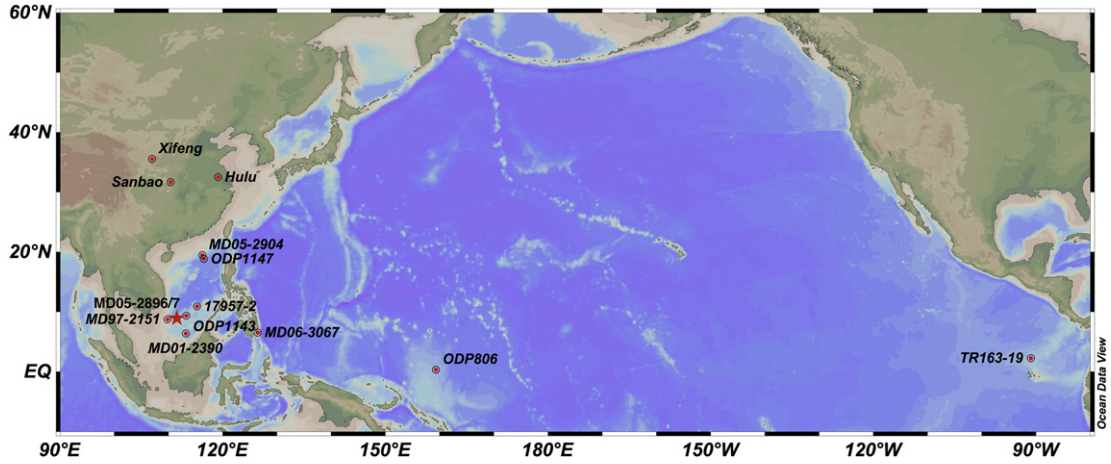

Figure 1. Overview map of the tropical Pacific Ocean, showing localities of sites mentioned in this study: ODP Site 1147 (Li et al., 2013), 17957-2 (Jian et al., 2000b), ODP Site 1143 (Tian et al., 2005), MD05-2896/7 (red star, this study), MD06-3067 (Bolliet et al., 2011), TR163-19 (Lea et al., 2000), MD97-2151 (Yamamoto et al., 2013), MD01-2390 (Steinke et al., 2010), ODP Site 806 (Lea et al., 2000), Xifeng Loess (Guo et al., 2009), Sanbao-Hulu Stalagmite (Cheng et al., 2012). The base map is from http://odv.awi.de.

5–30°C), and for SSST calculation, we use the equation calibrated by Jia et al. (2012): SSST = $(54.5 \pm 9.2) \times \mathrm{TEX}_{86}^{H} + (30.7 \pm 1.3)$ (r^2 0.79, n = 40, $p \ll 0.001$, 30–125 m).

Extraction of alkenone lipids and GC analysis

The other part of TLE was concentrated and then saponified with 3 ml of 6% KOH/methanol overnight. Neutral components were recovered by extraction with *n*-hexane four times, and then separated into non-polar and polar by silica gel column. The alkenone were measured using a Trace GC 2000 chromatograph (Finnigan, Thermo Electron) equipped with HP-1 capillary column (50 m × 0.32 mm × 0.17 μm, J&W) and flame ionization detector (FID). Both the injector and detector were set at 300°C. Hydrogen was used as the carrier gas with a flow rate of 1.2 ml/min by split-less injecting. The oven was kept initially at 60° C for 1 min, then was programmed from 80° C to

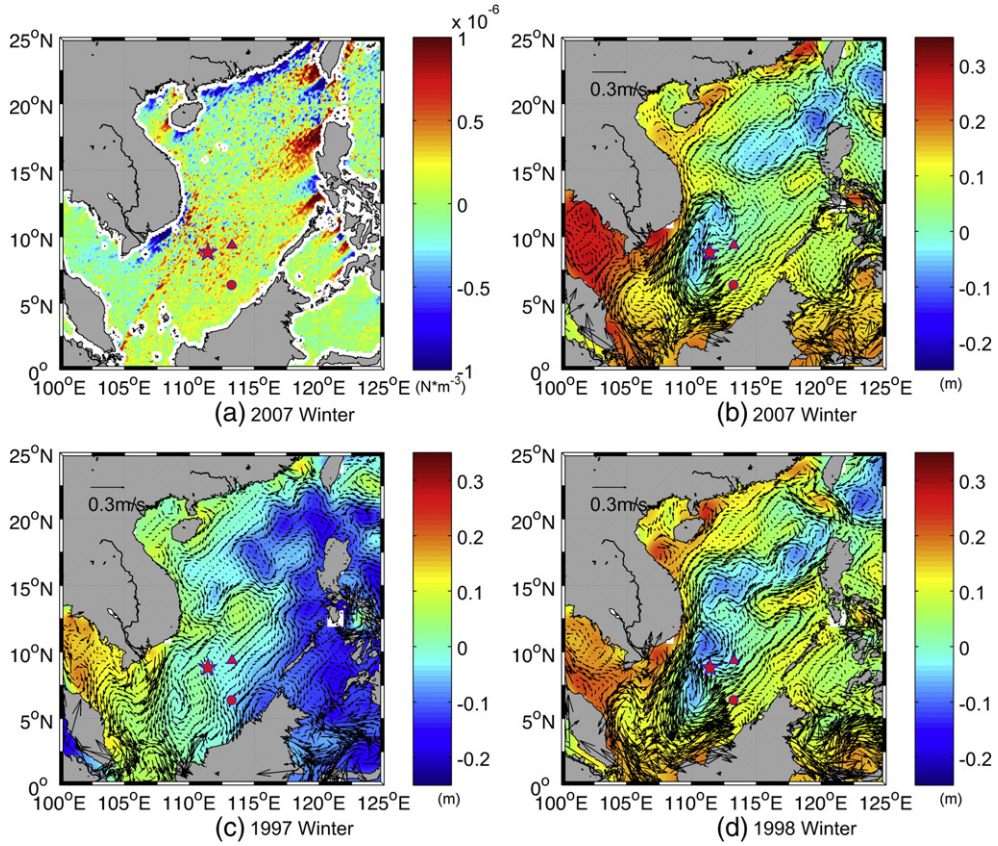

Figure 2. Modern oceanographic patterns in the SCS. (a) Seasonal wind stress curl (N/m^3) in 2007 winter (normal year) derived from QuikSCAT. (b, c, d) Sea-level anomaly (color bar) and geostrophic current (arrows) conditions in winter of 2007 (normal year), 1997 (El Niño), 1998 (La Niña), respectively. Also labeled are localities of MD05-2896/7 (red star), ODP1143 (red triangle) and MD01-2390 (red solid circle). Data from http://coastwatch.pfeg.noaa.gov/erddap/griddap/index.html?page=1&itemsPerPage=1000.

https://doi.org/10.1016/j.yqres.2014.12.003 Published online by Cambridge University Press

200° C at 10° C/min, followed by 5° C/min to 270° C, then 2° C/min to 300° C (maintained for 5 min), 5° C/min to 310° C (maintained for 5 min). Some of the samples were performed on GC-MS to confirm no co-eluting existence as the same GC program (Li et al., 2011).

$U^{K'}_{37}$ is defined as C37:2/(C37:3 + C37:2) (Brassell et al., 1986). For SST calculation, we follow the equation established by Pelejero and Grimalt (1997): SST = $(U^{K'}_{37} - 0.092)/0.031$ (r^2 0.86, n = 31, 0–30 m). Presumably, the results manifest the annual mean temperature in the 0–30 m mixed layer.

All the analyses and measurements were undertaken in the State Key Laboratory of Marine Geology at Tongji University.

Results

As shown in Figure 3, the $U^{K'}_{37}$-based SST (Fig. 3b) varied between 25 °C and 30° C, which followed the benthic foraminifer $\delta^{18}O$ curve (Fig. 3a) in displaying apparent glacial–interglacial cycles over the last 175 ka. As expected, a $U^{K'}_{37}$-SST maximum (29° C) occurred at MIS 5e and a minimum (24.8° C) at MIS 2, but $U^{K'}_{37}$-SST for MIS 6 varied between 26° C and 28° C, significantly higher than the values for MIS 2.

Based on the equation of Jia et al. (2012), TEX $^{H}_{86}$-derived SSST (Fig. 3d) averaged about 23° C for the Holocene and MIS 5e and ~20–21° C for MIS 2 and MIS 6. Generally, TEX $^{H}_{86}$-derived SSST was consistently lower by approximately 5° C than $U^{K'}_{37}$-derived SST. Compared to the $U^{K'}_{37}$-based SST, the TEX $^{H}_{86}$-based SSST curve matched better with the *P. obliquiloculata* Mg/Ca-derived SSST (Fig. 3c) of MD06-3067 located in the Philippine Sea, as shown by an overlap between the two SSST records especially for MIS 5. For other periods, such as MIS 3 and MIS 6, these records all ranged from ~20 to 24° C. In this study, therefore, the $U^{K'}_{37}$ result was chosen for representing SST and the TEX $^{H}_{86}$ result for SSST.

The differences between $U^{K'}_{37}$-derived SST and TEX $^{H}_{86}$-derived SSST were then used to calculate the DOT variations using an equation by Jia et al. (2012), which was originally defined for the depth of the 18 °C isothermal layer in the modern SCS. As shown in Figure 3, the difference between $U^{K'}_{37}$-derived SST and TEX $^{H}_{86}$-derived SSST (Fig. 3e) varied between ~4 and ~8° C, and the calculated DOT (Fig. 3f) fluctuated between ~100 and ~140 m. For MIS 5e and MIS 1, the SST-SSST difference was about 4° C, and the DOT was located at ~135 m. At warm to cold transitions MIS 3/2 and MIS 5/4, however, the SST–SSST difference increased to >7° C while DOT rose to ~110 m. Although many studies have demonstrated that warm climate often leads to relative low vertical thermal gradient and deeper thermocline, and vice versa for cold climate (Sagawa et al., 2012), the thermal gradient curve from core MD05-2897 (Fig. 3e) only loosely follows the typical glacial/interglacial features in the $\delta^{18}O$ curve. Specifically, the SST–SSST difference for MIS 3 is not as low as expected, and for MIS 6 it is even higher than expected.

Discussion

Patterns of DOT variability based on ΔT ($U^{K'}_{37}$ − TEX $^{H}_{86}$)

Based on modern surface water and core-top investigations in the SCS, the $U^{K'}_{37}$ has been found having a good relationship with the annual and winter SST (Pelejero and Grimalt, 1997) while the TEX_{86} or TEX $^{H}_{86}$-derived SST represent better the annual mean SST (Wei et al., 2011) or SSST (Jia et al., 2012). Because the branched/isoprenoid tetraethers (BIT index) values are always below 0.3, the influence of soil organic matter input on our TEX $^{H}_{86}$ record appears to be unlikely. By reference to Wei et al. (2011) and Jia et al. (2012) and to our own unpublished modern water measuring results, we assumed $U^{K'}_{37}$ and TEX $^{H}_{86}$ represent annual mean SST and SSST, respectively, which enable us to reconstruct DOT variation in core MD05-2896/7 using the $\Delta T_{(Alkenoe\text{-}GDGT)}$-based DOT calibration (Jia et al., 2012).

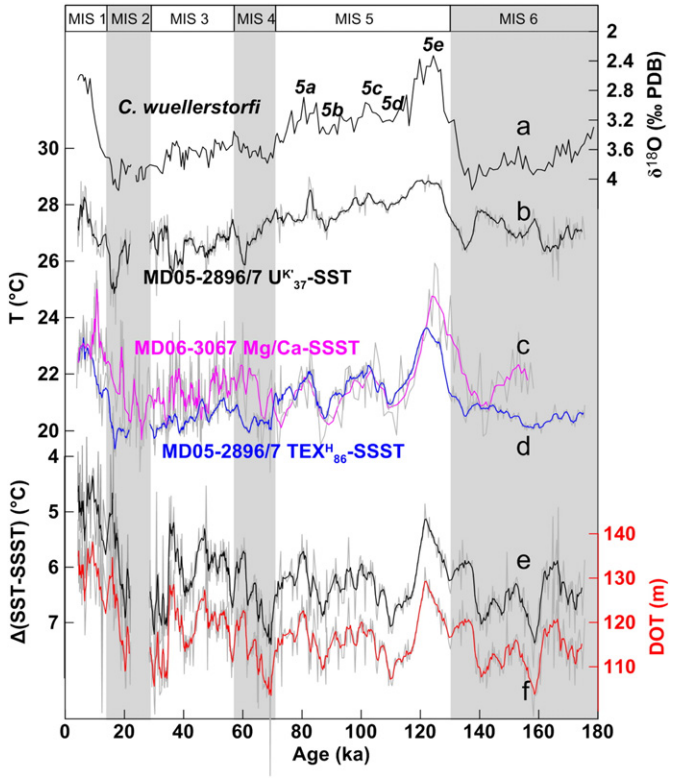

Figure 3. Oxygen isotope and temperature records over the last 175 ka from MD05-2896/7, southern SCS. (a) Benthic foraminifer species *Cibicidoides wuellerstorfi* $\delta^{18}O$ stratigraphy marked with Marine Isotope Stages (MIS) 1 to 6. (b) $U^{K'}_{37}$-derived annual mean sea-surface temperature (SST). (c) Mg/Ca-derived SST of MD06-3067 (red, Bolliet et al., 2011). (d) TEX $^{H}_{86}$-derived subsea surface temperature (SSST) of MD05-2896/7 based on equation from Jia et al., 2012 (blue). (e) Temperature difference (black) between $U^{K'}_{37}$-derived SST and TEX $^{H}_{86}$-derived SSST of MD05-2896/7. (f) Depth of thermocline (DOT) record (red) derived from the difference between $U^{K'}_{37}$-derived SST and TEX $^{H}_{86}$-derived SSST based on an equation by Jia et al. (2012). Thin lines and coarse lines represent the original data and the 5-point moving average, respectively.

The DOT results from core MD05-2896/7 (Fig. 4a) and the fauna-based thermocline record in core 17957-2 (10°53.09′N, 115°18.3′E; water depth 2195 m; Fig. 4b) (Jian et al., 2000b) both show similar deepening trends during early interglacial relative to glacial periods, and some obvious shoaling DOT events at MIS 5d, MIS 5/4 and MIS 3/2. However, the overall range of DOT in our record is shallower (100–140 m) compared to deeper range (140–200 m) in core 17957-2 (Fig. 4a,b). Especially for MIS 6, our record shows the DOT at 110–120 m, but it is 130–200 m based on faunal record in core 17957-2. These differences are likely caused not only by the two different methods employed, such as the seasonal production and exportation of GDGTs versus unsaturated alkenones, but also by the different geomorphological settings, such as the water depths between the two cores varying up to 500 m.

Interestingly, our results show similar changes with the *P. obliquiloculata* Mg/Ca-based thermocline temperature (Fig. 3c) in core MD06-3067 (6°31′N, 126°30′E, water depth: 1575 m) from the Philippine Sea (Bolliet et al., 2011). Based on temperature reconstruction using Mg/Ca in multi-species of planktonic foraminifera, Sagawa et al. (2012) studied the thermocline depth evolution in the WPWP and found that the thermocline in the Late Holocene was deeper than in the LGM, supporting the present scenario with deeper thermocline in the warmer West and shallower thermocline in the cooler East Pacific. Likewise, therefore, the DOT in the southern SCS as a whole

https://doi.org/10.1016/j.yqres.2014.12.003 Published online by Cambridge University Press

was likely deeper in interglacials but shallower in glacials, as found in our records from MD05-2896/7.

However, the ΔT between $U^{K'}_{37}$- and TEX $^{H}_{86}$-derived temperatures in our southern SCS core MD05-2896/7 and at ODP Site 1147 (Li et al., 2013) from the northern SCS with relative low-resolution shows distinct differences, which have most likely resulted from their different responses to driving factors such as EAWM. In the southern SCS, at ODP Site 1143 (9°21.720′N, 113°17.102′E; water depth 2771 m), a thermocline proxy record based on oxygen isotope difference between the subsurface dwelling planktonic foraminifer *P. obliquiloculata* and the surface species *G. ruber*, or $\Delta\delta^{18}O_{(P-G)}$ (Fig. 4c), has been generated (Tian et al., 2005). In particular, large values of $\Delta\delta^{18}O_{(P-G)}$ were used to indicate a shallow thermocline for warm intervals and their smaller values a deeper thermocline for cold intervals, thus revealing a completely opposite trend to faunal and our DOT records. As reported in many studies, *P. obliquiloculata* achieved abnormal high abundance during glacial periods in the southern SCS (e.g., Li et al., 2010; Xu et al., 2005), which may have affected the $\Delta\delta^{18}O_{(P-G)}$ and related signals. But it is not known whether the $\Delta\delta^{18}O_{(P-G)}$ results from ODP 1143 can be used to infer DOT changes as those originally detected from upwelling areas (Ravelo and Shackleton, 1995). Other factors, such as monsoon-related salinity and nutrient changes may have also disturbed the local $\Delta\delta^{18}O_{(P-G)}$ at ODP 1143 (Steinke et al., 2010). Nevertheless, the ΔSST-SSST-based DOT in core MD05-2896/7 and the fauna-based DOT in core 17957-2 (Jian et al., 2000b) show similar changes with shoaling DOT corresponding to smaller $\Delta\delta^{18}O_{(P-G)}$ values and deepening DOT to larger $\Delta\delta^{18}O_{(P-G)}$ values (Fig. 4).

Thermocline changes and East Asian Monsoon

Modern observation has confirmed that the DOT in the study area is driven by the regional wind stress curl, and the upper boundary of the thermocline could be uplifted by the positive wind stress curl especially during the Ekman upwelling in winter (Fig. 2a) (Liu et al., 2004). Leech et al. (2013) also illustrate this relationship between wind stress curl and DOT in their paleo-record from the western Pacific. As stated above, the DOT record from core MD05-2896/7 reveals a shoaling DOT in cold and glacial intervals and a depressed DOT in warm and interglacial intervals (Figs. 3 and 4), in contrast to the inferences by Tian et al. (2005) based on the $\Delta\delta^{18}O_{(P-G)}$ of ODP1143 and by Steinke et al. (2010) based on $\Delta T_{(P-G)}$ and alkenone records of MD01-2390. The $\Delta\delta^{18}O_{(P-G)}$ approach has been examined by Steinke et al. (2010) who found that a salinity effect could have influenced the $\Delta\delta^{18}O_{(P-G)}$. Furthermore, ODP 1143 is located at the margin of a modern winter cold eddy (Fig. 2), which could have contributed to some different response to monsoon and other hydroclimatic activities in the region, although the existence of the cold eddy throughout the late Quaternary glacial cycles was unlikely. For core MD01-2390, which is located far away from the cyclonic current caused by positive wind stress curl in winter (Fig. 2), its DOT record mirrors that of MD05-2896/7 in having a deeper DOT in the LGM and a shallower one in the Holocene. As revealed in our results, however, the scenario with a deeper DOT in the Holocene and other warm interval (Fig. 4a) is supported by modeling (Liu et al., 2002), which shows a maximum modeled vertical fluxes of dissolved inorganic nitrogen (DIN) area at 125 m water depth in the southwest SCS. The modeled maximum DIN area is consistent with the modern observed cold eddy area as shown in Figure 2, where an uplifted nutricline has long been observed (Gong et al., 1992). Based on the relative abundance of *Florisphaera profunda* in core MD05-2897, Su et al. (2013) found a shallower nutricline in the glacial period and a deeper nutricline in the interglacial period, corresponding to shoaling DOT and deepening DOT, respectively.

In the LGM period, the regional sea level fell by almost ~120 m, and a huge paleo-river network developed on the exposed paleo-Sunda Shelf and discharged large amounts of fresh water directly into the sea basin, which subsequently enhanced the stratification of the upper sea water (Li et al., 2010). For the southern SCS deep water, however, modern observation (Wang et al., 2011) and numerical study (Lan et al., 2013) both show a constant cyclonic circulation from 2000 m to bottom depths. Only strong monsoon would have neutralized the stratified water column and lifted the DOT.

In order to better understand the relationship between the DOT and EAM on the glacial–interglacial time scale, we compare our DOT record with two winter monsoon records (Fig. 5b, d) and the stalagmite $\delta^{18}O$-derived summer monsoon record (Fig. 5e) (Cheng et al., 2012; Wang et al., 2001; Wang et al., 2008), respectively. The winter monsoon records include the SST gradient between the northern and southern SCS (ΔSST_{N-S}) (Fig. 5b, this study), and the >32 μm grain size percentage from the loess plateau (Fig. 5d, Ding et al., 2002; Guo et al., 2009), although whether these proxies are robust indices of the EAM is still open to debate. The ΔSST_{N-S} as a winter monsoon proxy was developed by Jian et al. (2009) and endorsed by Tian et al. (2010), who demonstrated that the annual mean SST difference between the northern and southern SCS reveals a close relationship with EAWM strength, with greater ΔSST_{S-N} values indicating stronger EAWM and smaller values weaker EAWM. In the following, we present high-resolution ΔSST_{S-N} data between the southern core MD05-2896/7 and the northern core MD05-2904 (He et al., 2008) (Fig. 5b) using the above approach.

As shown in Figure 5, our DOT record from core MD05-2896/7 matches well with these winter monsoon proxies, with shoaling DOT mostly at times of strong winter monsoon. A long term stepwise DOT shoaling from 120 ka to 12 ka corresponds to a period of strengthened winter monsoon. Especially at 110, 90, 70, 55, 30 and 20 ka on the amplified ΔSST_{S-N} records (Fig. 5b), our reconstructed DOT in core MD05-2896/7 also became shallow (Fig. 5a), indicating the effect of enhanced winter monsoon on the upper water structure fluctuation in the southern SCS. These appear to support the hypothesis that the stronger the EAWM is, the shallower the DOT becomes, or vice versa for weaker EAWM. Such simple comparisons, however, cannot testify their credibility as good monsoon proxies or their common link to monsoon strength, as recent studies have revealed that winter and summer monsoons may not have been always acting inversely (Huang et al., 2011; Tian et al., 2010). Nevertheless, our DOT record

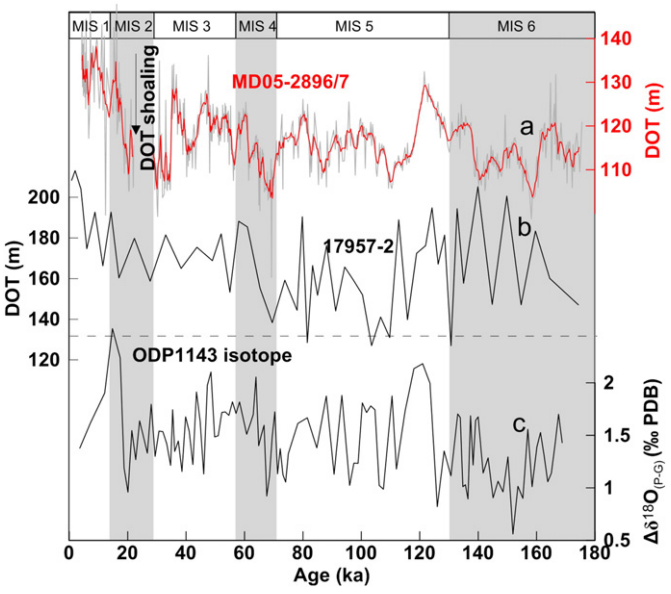

Figure 4. Comparison between different DOT records. (a) DOT record (red) of MD05-2896/7, as in Figure 3f. (b) DOT record of core 17957-2 based on foraminiferal transfer function (Jian et al., 2000b). (c) $\Delta\delta^{18}O_{(P-G)}$ record at ODP 1143 (Tian et al., 2005). Thin line and coarse line represent the original data and the 5-point moving average, respectively.

https://doi.org/10.1016/j.yqres.2014.12.003 Published online by Cambridge University Press

from core MD05-2896/7, at least for the Holocene part, is supported by the modern sea-level anomaly observation on a seasonal time scale, which shows that a constant cyclonic cold eddy develops around the core site by a positive wind stress curl due to the prevailing EAWM and subsequently uplifts the DOT.

Similar to these monsoon proxies, our reconstructed DOT shows clear millennial-scale frequency changes (Fig. 5a). Early MIS 2 (around 20 ka) and MIS 6 (around 160 ka) are two time periods when strong winter (Fig. 5b) and summer monsoons (Fig. 5e) coincided with a shallow DOT, implying that the EAWM dominates the pattern of the DOT variation. At the MIS 6/5 and MIS 2/1 boundaries, although the EASM was implied by proxies as enhanced sharply, the gradually weakenning winter monsoon was associating with a slowly deepening DOT, also supporting the EAWM dominance on the DOT variation. During the H1 cooling event around 18 ka, the sharply deepening DOT corresponded to a weakened EAWM, when EASM was also much weaker. Therefore, all these imply that the strengthed EAWM has been the main control factor for the shoaling of the DOT in the studied region.

Apart from the monsoon, however, other hydroclimatic factors such as the El Niño-Southern Oscillation (ENSO) may have exerted influence on the upper ocean thermal structure in the SCS due to its linkage with the warm pool. Studies have shown that the seasonal wind pattern could be driven by ENSO variability, as boreal winter monsoon often reduces during El Niño events while boreal summer monsoon weakens during La Niña periods (Sakai and Kawamura, 2009; Wang et al., 2000). In the following we will explore the possibility of influence by ENSO-like dynamics on DOT variations on the glacial–interglacial time scale.

DOT variability as related to ENSO-like dynamics

ENSO is an extraordinary hydrological feature across the tropical Pacific, with the normal state characterized by very high SSTs and a thick and deep thermocline (~130 m) in the west, but relatively low SSTs and thin and shallower thermocline in the east because of strong upwelling. These hydrological patterns often become strengthened at the La Niña state or weakened at the El Niño state, with oscillations of 2–7 yr. Generally, the SST gradient between the western and eastern tropical Pacific ($\Delta SST_{W\text{-}E}$) has been widely used to infer the variation of El Niño-like (low $\Delta SST_{W\text{-}E}$) and La Niña-like (high $\Delta SST_{W\text{-}E}$) conditions over various time periods (e.g., Koutavas et al., 2002; Shaari et al, 2013).

To explore for the evidence of ENSO changes, we examined the Mg/Ca-derived SST difference between ODP 806B in the open WPWP (159°22′W, 0°19′N, water depth 2520 m) and core TR163-19 from the eastern Pacific (90°57.04′W, 2°15.18′N, water depth 2348 m) (Lea et al., 2000), or $\Delta SST_{(ODP806B\text{-}TR163\text{-}19)}$ (Fig. 5c). The $\Delta SST_{W\text{-}E}$ results show a mean zonal thermal gradient of ~1.8° C for interglacial and warm intervals, but 3.5° C for glacial and cold intervals, indicating that the zonal wind stress (Walker circulation) was intensified during the glacial periods as found in many previous studies (e.g., Andreasen and Ravelo, 1997; Li et al., 2011). Although the sampling time resolution does not permit direct deduction of El Niño or La Niña events over the last 175 ka, these $\Delta SST_{W\text{-}E}$ records can still provide crucial information on the tropical Pacific hydroclimate variability (e.g., Koutavas et al., 2002; Lea et al., 2000). Accordingly, the relatively increased $\Delta SST_{W\text{-}E}$ over the glacials is considered inferable for a La Niña-like state with increasing frequency of La Niña activities. These La Niña-like states were mainly caused by the enhanced trade wind, which may also have intersected and strengthened the EAWM. Subsequently, the positive wind stress curl in winter driven by both the enhanced monsoon and intensified trade wind would become stronger and raise the DOT. Remarkable is that the $\Delta SST_{S\text{-}N}$, $\Delta SST_{W\text{-}E}$ and $\Delta SST_{SST\text{-}SSST}$ for MIS 3 and 4 all appear to become smaller than those for LGM, which may reflect a weaker EAWM and enhanced El Niño activities in most part of the last glacial period except LGM with strengthened winter monsoon. Similar phenomena can also be observed across MIS5/4, MIS2/1 and MIS6/5 boundaries (Fig. 5). Enhanced El Niño-like activities during most part of the last glacial interval have found support from studies of the Celebes Sea by Bolliet et al. (2011) and the eastern equatorial Pacific by Leduc et al. (2009).

Therefore, one basic feature revealed by many studies is that the WPWP shrank (expanded) during the glacial (interglacial) periods, as deduced by the increase (reduction) of zonal, meridional and vertical thermal gradients of the WPWP in the glacial (interglacial) periods. As a response during glacial periods, the northeast trade winds could enhance the EAWM, which in turn may strengthen upwelling and uplift the DOT in the southern SCS.

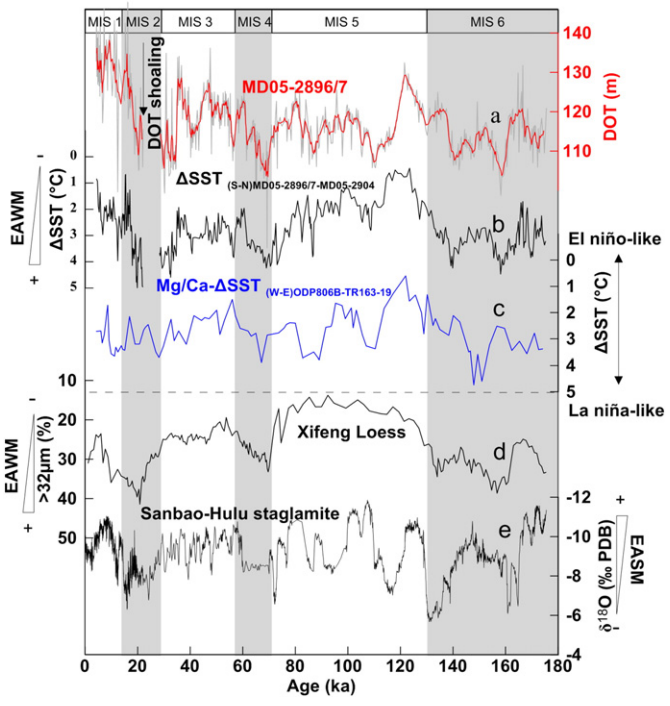

Figure 5. Comparison between DOT, EAM and ENSO records. (a) DOT record (red) of MD05-2896/7, as in Figure 3f. (b) Meridional SST difference $\Delta SST_{S\text{-}N}$ (black) between southern (MD05-2896/7) and northern (MD05-2904, He et al., 2008) SCS. (c) Zonal SST difference $\Delta SST_{W\text{-}E}$ (blue) between WPWP (ODP 806B) and eastern Pacific (TR163-19, Lea et al., 2000). (d) East Asian winter monsoon record based on >32 μm loess grain size from Xifeng, China (Guo et al., 2009). (e) East Asian summer monsoon record derived from the stalagmite $\delta^{18}O$ at Hulu-Sanbao cave (black, Cheng et al., 2012). Coarse red line in (a) represents the 5-point moving average; all other lines represent the original data.

Conclusions

The differences between the $U^{K'}_{37}$-derived SST and TEX $^{H}_{86}$-derived SSST in core MD05-2896/7 are used to reflect variations in upper thermocline depth in the southern SCS over the last 175 ka. Our results indicate that the upper water structure at this site has been sensitively responding to EAWM and Pacific ENSO-like hydrodynamics over glacial-interglacial cycles. The reconstructed DOT record provides evidence of the influence of both the EAWM and ENSO-like conditions, with stronger EAWM and La Niña states leading to thermocline shoaling particularly during glacial and cold periods. However, the behavior of short-term DOT variation in different parts of the SCS still awaits further investigations.

Acknowledgments

We appreciate the help of the crew onboard the R/V *Marion Dufresne* during the MD147-Marco-Polo Cruise in 2005. We thank Jun Tian and Enqing Huang for providing the benthic oxygen isotope data of MD05-

2896/7, and Zhonghui Liu, Bangqi Hu and Jiangnan Shi for insightful discussion. The two anonymous reviewers and the Associate Editor handling this paper are thanked for constructive comments, which greatly improved an earlier version of the manuscript. This research was supported by the Ministry of Science and Technology of China (2013CB955704), the National Natural Science Foundation of China (41076017, 91028005, 91228203), the "National Thousand Talents Program" at Tongji University (CLZ), and Innovation Program of Shanghai Municipal Education Commission (12ZZ031).

References

Andreasen, D., Ravelo, A., 1997. Tropical Pacific Ocean thermocline depth reconstructions for the last glacial maximum. Paleoceanography 12, 395–413.
Andreasen, D.H., Ravelo, A.C., Broccoli, A.J., 2001. Remote forcing at the Last Glacial Maximum in the tropical Pacific Ocean. Journal of Geophysical Research 106, 879–897.
Beaufort, L., de Garidel-Thoron, T., Mix, A.C., Pisias, N.G., 2001. ENSO-like forcing on oceanic primary production during the late Pleistocene. Science 293, 2440–2444.
Beaufort, L., de Garidel-Thoron, T., Linsley, B., Oppo, D., Buchet, N., 2003. Biomass burning and oceanic primary production estimates in the Sulu Sea area over the last 380 kyr and the East Asian monsoon dynamics. Marine Geology 201, 53–65.
Bolliet, T., Holbourn, A., Kuhnt, W., Laj, C., Kissel, C., Beaufort, L., Kienast, M., Andersen, N., Garbe-Schönberg, D., 2011. Mindanao Dome variability over the last 160 ka: episodic glacial cooling of the West Pacific Warm Pool. Paleoceanography 26, PA1208.
Brassell, S., Eglinton, G., Marlowe, I., Pflaumann, U., Sarnthein, M., 1986. Molecular stratigraphy: a new tool for climatic assessment. Nature 320, 129–133.
Cheng, H., Zhang, P., Spötl, C., Edwards, R., Cai, Y., Zhang, D., Sang, W., Tan, M., An, Z., 2012. The climatic cyclicity in semiarid-arid central Asia over the past 500,000 years. Geophysical Research Letters 39, L01705.
Ding, Z., Ranov, V., Yang, S., Finaev, A., Han, J., Wang, G., 2002. The loess record in southern Tajikistan and correlation with Chinese loess. Earth Planetary Science Letters 200, 387–400.
Gong, G.-C., Liu, K.K., Liu, C.-T., Pai, S.-C., 1992. The chemical hydrography of the South China Sea west of Luzon and a comparison with the West Philippine Sea. Terrestrial, Atmospheric and Oceanic Sciences 3, 587–602.
Guo, Z., Berger, A., Yin, Q., Qin, L., 2009. Strong asymmetry of hemispheric climates during MIS-13 inferred from correlating China loess and Antarctica ice records. Climate of Past 5, 21–31.
He, S., Wang, H., 2013. Oscillating relationship between the East Asian winter monsoon and ENSO. Journal of Climate 26, 9819–9838.
He, J., Zhao, M.X., Li, L., Wang, P.X., Ge, H.M., 2008. Sea-surface temperature and terrestrial biomarker records of the last 260 ka of core MD05-2904 from the northern South China Sea. Chinese Science Bulletin 53, 2376–2384.
Hopmans, E.C., Weijers, J.W.H., Schefuβ, E., Herfort, L., Sinninghe Damsté, J.S., Schouten, S., 2004. A novel proxy for terrestrial organic matter in sediments based on branched and isoprenoid tetraether lipids. Earth Planetary Science Letters 224, 107–116.
Hu, A., Jiao, N., Zhang, C.L., 2011. Community structure and function of planktonic Crenarchaeota: changes with depth in the South China Sea. Microbial Ecology 62, 549–563.
Huang, E., Tian, J., 2012. Sea-level rises at Heinrich stadials of early Marine Isotope Stage 3: evidence of terrigenous n-alkane input in the southern South China Sea. Global and Planetary Change 94, 1–12.
Huang, E., Tian, J., Steinke, S., 2011. Millennial-scale dynamics of the winter cold tongue in the southern South China Sea over the past 26 ka and the East Asian winter monsoon. Quaternary Research 75, 196–204.
Jia, G.D., Zhang, J., Chen, J.F., Peng, P.A., Zhang, C.L., 2012. Archaeal tetraether lipids record subsurface water temperature in the South China Sea. Organic Geochemistry 50, 68–77. http://dx.doi.org/10.1016/j.orggeochem.2012.07.002.
Jian, Z.M., Li, B.H., Huang, B.Q., Wang, J.L., 2000a. *Globorotalia truncatulinoides* as indicator of upper-ocean thermal structure during the Quaternary: evidence from the South China Sea and Okinawa Trough. Palaeogeography, Palaeoclimatology, Palaeoecology 162, 287–298.
Jian, Z.M., Wang, P.X., Chen, M.-P., Li, B.H., Zhao, Q.H., Bühring, C., Laj, C., Lin, H.-L., Pflaumann, U., Bian, Y.H., Wang, R.J., Cheng, X.R., 2000b. Foraminiferal responses to major Pleistocene paleoceanographic changes in the southern South China Sea. Paleoceanography 15, 229–243.
Jian, Z., Tian, J., Sun, X., 2009. Upper Water Structure and Paleo-Monsoon. In: Wang, P.X., Li, Q.Y. (Eds.), The South China Sea: Paleoceanography and Sedimentology. Springer, Netherlands, pp. 297–394.
Karner, M.B., DeLong, E.F., Karl, D.M., 2001. Archaeal dominance in the mesopelagiczone of the Pacific Ocean. Nature 409, 507–510.
Kim, J.-H., Schouten, S., Hopmans, E.C., Donner, B., Sinninghe Damsté, J.S., 2008. Global sediment core-top calibration of the TEX_{86} paleothermometer in the ocean. Geochimica et Cosmochimica Acta 72, 1154–1173.
Kim, J.-H., van der Meer, J., Schouten, S., Helmke, P., Willmott, V., Sangiorgi, F., Koç, N., Hopmans, E.C., Damsté, J.S.S., 2010. New indices and calibrations derived from the distribution of crenarchaeal isoprenoid tetraether lipids: implications for past sea-surface temperature reconstructions. Geochimica et Cosmochimica Acta 74, 4639–4654.
Koutavas, A., Joanides, S., 2012. El Niño–Southern Oscillation extrema in the Holocene and Last Glacial Maximum. Paleoceanography 27, PA4208.
Koutavas, A., Lynch-Stieglitz, J., Marchitto, T.M., Sachs, J.P., 2002. El Niño-like pattern in ice age tropical Pacific sea-surface temperature. Science 297, 226–230.
Koutavas, A., Olive, G.C., Lynch-Stieglitz, J., 2006. Mid-Holocene El Niño–Southern Oscillation (ENSO) attenuation revealed by individual foraminifera in eastern tropical Pacific sediments. Geology 34, 993–996.
Laj, C., Wang, P., Balut, Y., 2005. IPEV les rapports de campagnes à la mer. MD147/MARCO POLO-IMAGES XIIà bord du "Maion Dufresne" (59 pp.).
Lan, J., Zhang, N., Wang, Y., 2013. On the dynamics of the South China Sea deep circulation. Journal of Geophysical Research, Oceans 118, 1206–1210.
Lea, D.W., Pak, D.K., Spero, H.J., 2000. Climate impact of late Quaternary equatorial Pacific sea surface temperature variations. Science 289, 1719–1724.
Leduc, G., Vidal, L., Cartapanis, O., Bard, E., 2009. Modes of eastern equatorial Pacific thermocline variability: implications for ENSO dynamics over the last glacial period. Paleoceanography 24, PA3202.
Leech, P.J., Lynch-Stieglitz, J., Zhang, R., 2013. Western Pacific thermocline structure and the Pacific marine Intertropical Convergence Zone during the Last Glacial Maximum. Earth Planetary Science Letters 363, 133–143.
Li, Q.Y., Zheng, F., Chen, M.H., Xiang, R., Qiao, P.J., Shao, L., Cheng, X.R., 2010. Glacial paleoceanography off the mouth of the Mekong River, southern South China Sea, during the last 500 ka. Quaternary Research 73, 563–572.
Li, L., Li, Q.Y., Tian, J., Wang, P.X., Wang, H., Liu, Z.H., 2011. A 4-Ma record of thermal evolution in the tropical western Pacific and its implications on climate change. Earth Planetary Science Letters 309, 10–20.
Li, D.W., Zhao, M.X., Tian, J., Li, L., 2013. Comparison and implication of TEX_{86} and $U^{K'}_{37}$ temperature records over the last 356 ka of ODP Site 1147 from the northern South China Sea. Palaeogeography, Palaeoclimatology, Palaeoecology 376, 213–223.
Lisiecki, L.E., Raymo, M.E., 2005. A Pliocene-Pleistocene stack of 57 globally distributed benthic $\delta^{18}O$ records. Paleoceanography 20, PA1003. http://dx.doi.org/10.1029/2004PA001071.
Liu, K.-K., Chao, S.-Y., Shaw, P.-T., Gong, G.-C., Chen, C.-C., Tang, T., 2002. Monsoon-forced chlorophyll distribution and primary production in the South China Sea: observations and a numerical study. Deep Sea Research Part I: Oceanographic Research 49, 1387–1412.
Liu, Q., Jiang, X., Xie, S.P., Liu, W.T., 2004. A gap in the Indo-Pacific warm pool over the South China Sea in boreal winter: seasonal development and interannual variability. Jounarl of Geophysical Research 109, C07012. http://dx.doi.org/10.1029/2003JC002179.
Liu, Z., Pagani, M., Zinniker, D., Deconto, R., Huber, M., Brinkhuis, H., Shah, S.R., Leckie, R.M., Pearson, A., 2009. Global cooling during the Eocene-Oligocene climate transition. Science 323, 1187–1190.
Lopes dos Santos, R.A., Prange, M., Castañeda, I.S., Schefuß, E., Mulitza, S., Schulz, M., Niedermeyer, E.M., Sinninghe Damsté, J.S., Schouten, S., 2010. Glacial–interglacial variability in Atlantic meridional overturning circulation and thermocline adjustments in the tropical North Atlantic. Earth Planetary Science Letters 300, 407–414.
Pelejero, C., Grimalt, J.O., 1997. The correlation between the U^{K}_{37} index and sea surface temperatures in the warm boundary: the South China Sea. Geochimica et Cosmochimica Acta 61, 4789–4797.
Picaut, J., Ioualalen, M., Menkès, C., Delcroix, T., McPhaden, M., 1996. Mechanism of the zonal displacements of the Pacific warm pool: implications for ENSO. Science 274, 1486–1489.
Ravelo, A., Fairbanks, R., 1992. Oxygen isotopic composition of multiple species of planktonic foraminifera: recorders of the modern photic zone temperature gradient. Paleoceanography 7, 815–831.
Ravelo, A., Shackleton, N., 1995. Evidence for surface-water circulation changes at Site 851 in the eastern tropical Pacific Ocean. Proceedings of the Ocean Drilling Program, Scientific Results 138, 503–514.
Sagawa, T., Yokoyama, Y., Ikehara, M., Kuwae, M., 2012. Shoaling of the western equatorial Pacific thermocline during the last glacial maximum inferred from multispecies temperature reconstruction of planktonic foraminifera. Palaeogeography, Palaeoclimatology, Palaeoecology 346, 120–129.
Sakai, K., Kawamura, R., 2009. Remote reponse of the East Asian winter monsoon to tropical forcing related to El Nino-Southern Oscillation. Journal of Geophysical Research: Atmoshperes 114, D06105. http://dx.doi.org/10.1029/2008JD010824.
Schouten, S., Hopmans, E., Schefuß, E., Damste, J.S.S., 2002. Distributional variations in marine crenarchaeotal membrane lipids: a new tool for reconstructing ancient sea water temperatures? Earth Planetary Science Letters 204, 265–274.
Schouten, S., Huguet, C., Hopmans, E.C., Kienhuis, M.V.M., Sinninghe Damsté, J.P., 2007. Analytical methodology for TEX_{86} paleothermometry by high-performance liquid chromatography/atmospheric pressure chemical ionization-mass spectrometry. Analytical Chemistry 79, 2940–2944.
Shaari, H., Yamamoto, M., Irino, T., 2013. Enhanced upwelling in the eastern equatorial Pacific at the last five glacial teminations. Palaeogeography, Palaeoclimatology, Palaeoecology 386, 8–15.
Shaari, H., Yamamoto, M., Irino, T., Oba, T., 2014. Nutricline shoaling in the eastern Pacific warm pool during the last two glacial maxima. Journal of Oceanography 70, 25–34.
Steinke, S., Mohtadi, M., Groeneveld, J., Lin, L.C., Löwemark, L., Chen, M.T., Rendle-Bühring, R., 2010. Reconstructing the southern South China Sea upper water column structure since the Last Glacial Maximum: implications for the East Asian winter monsoon development. Paleoceanography 25 PA2219.
Steinke, S., Glatz, C., Mohtadi, M., Groeneveld, J., Li, Q., Jian, Z., 2011. Past dynamics of the East Asian monsoon: no inverse behaviour between the summer and winter monsoon during the Holocene. Global and Planetary Change 78, 170–177.
Stott, L., Poulsen, C., Lund, S., Thunell, R., 2002. Supper ENSO and global climate oscillations at millennial time scales. Science 297, 222–226.

https://doi.org/10.1016/j.yqres.2014.12.003 Published online by Cambridge University Press

Su, X., Liu, C., Beaufort, L., Tian, J., Huang, E., 2013. Late Quaternary coccolith records in the South China Sea and East Asian monsoon dynamics. Global and Planetary Change 111, 88–96.
Tian, J., Wang, P., Chen, R., Cheng, X., 2005. Quaternary upper ocean thermal gradient variations in the South China Sea: implications for East Asian monsoon climate. Paleoceanography 20, PA4007.
Tian, J., Huang, E., Pak, D.K., 2010. East Asian winter monsoon variability over the last glacial cycle: insights from a latitudinal sea-surface temperature gradient across the South China Sea. Palaeogeography, Palaeoclimatology, Palaeoecology 292, 319–324.
Tudhope, A.W., Chilcott, C.P., McCulloch, M.T., Cook, E.R., Chappell, J., Ellam, R.M., Lea, D.W., Lough, J.M., Shimmield, G.B., 2001. Variability in the El Niño-southern oscillation through a glacial-interglacial cycle. Science 291, 1511–1517.
Wang, P.X., Li, Q.Y., 2009. The South China Sea: paleoceanography and Sedimentology. Springer, Netherlands.
Wang, B., Wu, R.G., Fu, X.H., 2000. Pacific-East Asian teleconnection: how does ENSO affect East Asian climate? Journal of Climate 12, 1517–1536.
Wang, Y.J., Cheng, H., Edwards, R.L., An, Z.S., Wu, J.Y., Shen, C.-C., Dorale, J.A., 2001. A high-resolution absolute-dated Late Pleistocene monsoon record from Hulu Cave, China. Science 294, 2345–2348.
Wang, P.X., Clemens, S., Beaufort, L., Braconnot, P., Ganssen, G., Jian, Z.M., Kershaw, P., Sarnthein, M., 2005. Evolution and variability of the Asian monsoon system: state of the art and outstanding issues. Quaternary Science Reviews 24, 595–629.
Wang, Y.J., Cheng, H., Edwards, R.L., Kong, X., Shao, X., Chen, S., Wu, J., Jiang, X., Wang, X., An, Z., 2008. Millennial- and orbital-scale changes in the East Asian monsoon over the past 224,000 years. Nature 451, 1090–1093.
Wang, G., Xie, S.P., Qu, T., Huang, R.X., 2011. Deep South China Sea circulation. Geophysical Research Letters 38, L05601.
Wang, L., Li, J.J., Lu, H.Y., Gu, Z.Y., Rioual, P., Hao, Q.Z., Mackay, A.W., Jiang, W.Y., Cai, B.G., Xu, B., Han, J.T., Chu, G.Q., 2012. The East Asian winter monsoon over the last 15,000 years: its links to high-latitudes and tropical climate systems and complex correlation to the summer monsoon. Quaternary Science Reviews 32, 131–142.
Wei, Y., Wang, J., Liu, J., Dong, L., Li, L., Wang, H., Wang, P., Zhao, M., Zhang, C.L., 2011. Spatial variations in archaeal lipids of surface water and core-top sediments in the South China Sea and theirimplications for paleoclimate studies. Applied and Environmental Microbiology 77, 7479–7489.
Wuchter, C., Schouten, S., Wakeham, S.G., Damsté, J.S.S., 2005. Temporal and spatial variation in tetraether membrane lipids of marine Crenarchaeota in particulate organic matter: implications for TEX_{86} paleothermometry. Paleoceanography 20, 1–11.
Xu, J., Wang, P.X., Huang, B.Q., Li, Q.Y., Jian, Z.M., 2005. Response of planktonic foraminifera to glacial cycles: Mid-Pleistocene change in the southern South China Sea. Marine Micropaleontology 54, 89–105.
Yamamoto, M., Sai, H., Chen, M.-T., Zhao, M., 2013. The East Asian winter monsoon variability in response to precession during the past 150 000 yr. Climate of Past 9, 2777–2788.
Zhao, M., Huang, C.Y., Wang, C.C., Wei, G., 2006. A millennial-scale U^{K}_{37} sea-surface temperature record from the South China Sea (8° N) over the last 150 kyr: monsoon and sea-level influence. Palaeogeography, Palaeoclimatology, Palaeoecology 236, 39–55.

https://doi.org/10.1016/j.yqres.2014.12.003 Published online by Cambridge University Press